Lithofacies and Diagenetic Features of Strawn Carbonates in the Subsurface of North-Central Texas: Implications to Controls on Reservoir Quality

Qilong Fu and William A. Ambrose

Bureau of Economic Geology, Jackson School of Geosciences, University of Texas at Austin, University Station, Box X, Austin, Texas 78713–8924, U.S.A.

ABSTRACT

The Strawn succession in the subsurface of north-central Texas contains many carbonate and siliciclastic hydrocarbon reservoirs. Our current study, which is on the basis of cores and thin sections, demonstrates that carbonate reservoirs consist mainly of bioclast wackestones to mud-rich packstones that we interpret to have been deposited in the middle-ramp setting and that represent the upper unit (regressive part) of individual cycle sets. Reservoir-quality pores are not observed in other carbonate lithofacies. Secondary vugs and molds are the dominant pore type, but residual interparticle and intragranular pores and dissolution-enhanced matrix pores are locally abundant. Vuggy and moldic pores are interpreted to have resulted from extensive freshwater-related leaching of carbonate grains (mainly bioclasts) and matrix during sea-level falls.

INTRODUCTION

Many oil fields have been developed in King County and adjacent counties in north-central Texas. The Pennsylvanian (Desmoinesian) Strawn Group is one of the major productive intervals. Exploration drilling had marginal success in the 1950s and 1960s, but in the 1970s primary production sharply increased after discovery of some major oil fields (e.g., the Burnett Ranch Field) in the area (Lee, 2019). Secondary production efforts began in the 1980s, and tertiary production started in 2010s. CO_2 floods are currently used to create higher pressure in the down-dip reservoirs to keep the CO_2 inside the hydrocarbon-bearing part of the reservoirs (Lee, 2019).

The Pennsylvanian (Desmoinesian) Strawn Group consists of cyclic carbonate and siliciclastic deposits on the northern Eastern Shelf, and siliciclastic delta facies interfinger with platform carbonate facies in King County (Boring, 1993; Cleaves, 2000). Carbonates were deposited on the Spur Platform along the northern edge of the Knox-Baylor Trough in the northern part of King County. This trough also extends to southeastern King County (Boring, 1993). The carbonate reservoirs studied herein are on the Spur Platform in northern King County and in Kent County to the southwest (Fig. 1).

Despite a relatively long history of exploration and exploitation of these prolific reservoirs (Lee, 2019), few detailed studies of the Strawn limestones in the subsurface of north-central Texas have been published. This study will (1) describe the carbonate lithofacies recognized in cores and thin sections and interpret their depositional environments, (2) investigate diagenetic history and pore evolution, and (3) evaluate relationships among pore networks, facies, and diagenetic elements, in order to characterize the heterogeneous carbonate reservoirs in the study area.

GEOLOGICAL SETTING

During the Desmoinesian, the Eastern Shelf of the Permian Basin (comprised of two major sub-basins: Midland Basin and Delaware Basin) was a low-gradient carbonate ramp (Yancey, 1986). This ramp system existed until the Missourian, when the Midland Basin subsided and a distinct shelf-slope system formed (Cleaves and Erxleben, 1985). Across the Knox-Baylor Trough, aggradational carbonates were deposited in the Red River Uplift (Fig. 1). The platform in King County (Spur Platform) represents a southward extension of the Matador Arch and Red River Uplift (Cleaves, 2000).

The Knox-Baylor Trough was a relatively shallow basin of middle and late Desmoinesian age (Gunn, 1979). It existed south of the Red River Uplift and northwest of the Concho Platform, and was connected to the eastern part of the Midland Basin in Mitchell and Fisher counties (Fig. 1B). King and Kent counties were near the axis of the Knox-Baylor Trough, which funneled siliciclastic sediments from the Wichita-Arbuckle mountains belt (Gunn, 1979; Lee, 2019). The Haskell delta system prograded episodically along the Knox-Baylor Trough (Fig. 1B). Terrestrial

Figure 1. Paleogeographic map showing structural elements of north-central and West Texas during the Desmoinesian (A) as well as major siliciclastic and carbonate depositional systems of the middle Strawn Group in north-central Texas (B). Modified after Gunn (1979), Cleaves (1993, 2000) and Wright (2011). Boundaries of the Permian Basin are modified after Hills (1984).
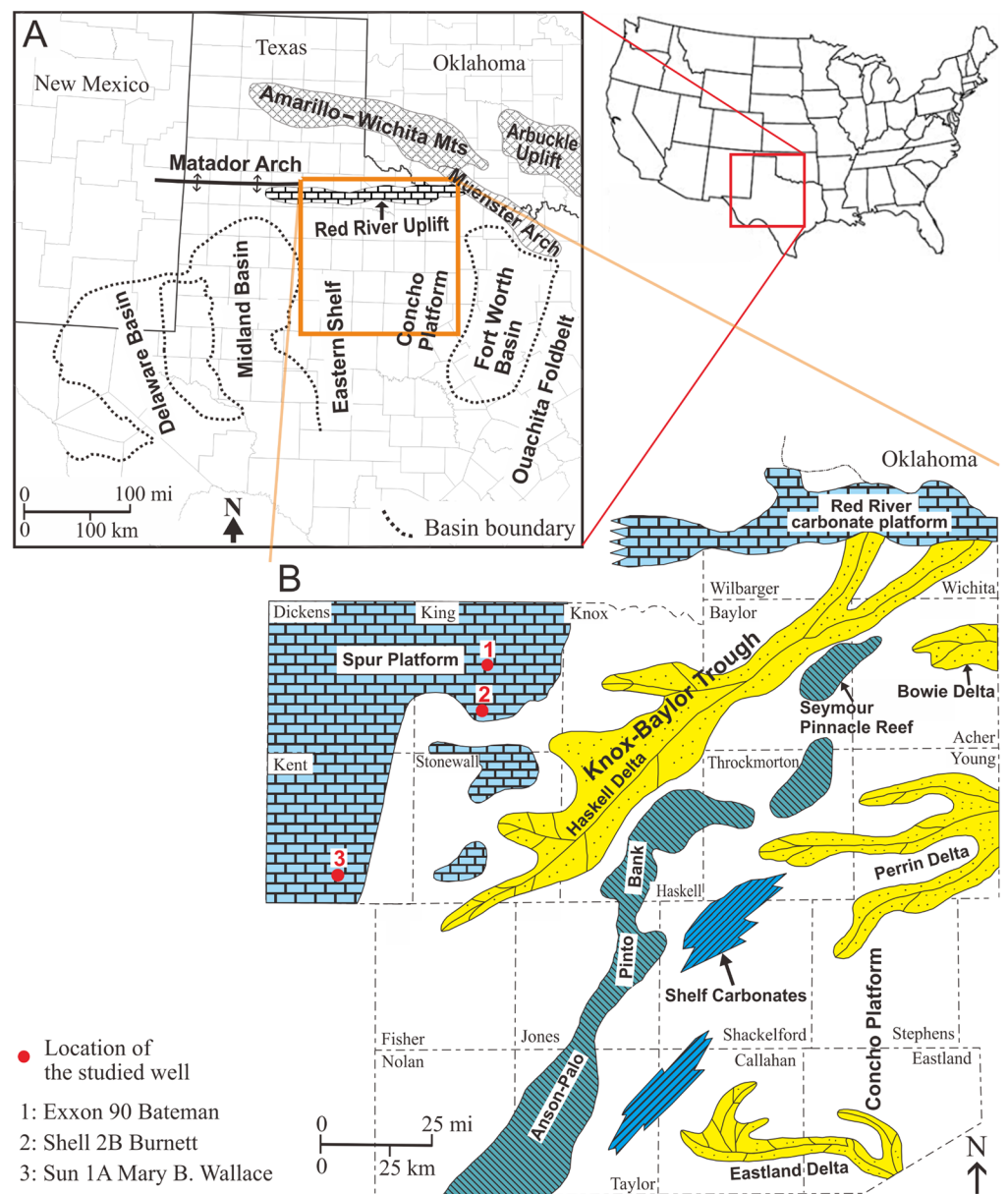
sediment supply and deltaic progradation on the Eastern Shelf was controlled by continued convergence of the Ouachita Thrust Belt to the east and southeast of the Fort Worth Basin (Cleaves, 1993). The distribution of siliciclastic and carbonate facies in the study area were highly impacted by progradation and retrogradation of the Haskell delta system along the Knox-Baylor Trough.

Strawn strata overlie the Atoka Group and are overlain by the Canyon Group (Fig. 2). The Strawn consists of the upper Caddo Limestone, upper Smithwick Shale (Strawn shale), Strawn (5400) limestone, Tandy 5400 (Katz 5100) sandstone, Anne Tandy siliciclastic rocks, and Twin Peaks sandstone (Gunn, 1979; Boring, 1993; Lee, 2019). The current study focuses on the Strawn (5400) limestone.

Cyclothemic deposition composed of siliciclastics and carbonates is recognized in the Pennsylvanian strata (including the Strawn Group). Glacio-eustatic sea level fluctuations were considered to be the dominant control on the cyclic deposition and facies distribution in the Eastern Shelf (Heckel, 1986, 1995; Marquis and Laury, 1989). Overall second-order transgression was punctuated by numerous high-frequency, high-amplitude, third-order (as well as higher order, lower-amplitude) regressive and

transgressive events (Haq and Schutter, 2008; Heckel, 2008). The maximum magnitude of third-order eustatic variation in sea level is estimated at approximately 120 m (394 ft) from the Desmoinesian to the Virgilian (Heckel, 2008; Rygel et al., 2008), and fourth-order sea-level fluctuations probably varied 20 to 130 ft (~6 to 40 m) (Ross and Ross, 2003).

Sequence stratigraphic analysis of the Strawn Group indicates that the cyclothemic deposits contain many disconformities and represent type 1 sequences (Cleaves, 1993, 2000). Reciprocal sedimentation was the dominant depositional pattern on the mixed carbonate-siliciclastic Eastern shelf. The distribution of carbonate facies across the Concho Platform–Eastern Shelf during the Desmoinesian was directly related to both the platform evolution and the availability of terrigenous clastic sediments (Cleaves, 2000). During eustatic transgressions and early highstands carbonates were deposited in a significant quantity. Progradational regression might bring about extensive river-dominated deltaic sedimentation during late highstands, prevented thick carbonate buildups from developing in places on the Eastern shelf (Cleaves, 2000). Major eustatic drops in sea level caused forced regressions, and the Eastern Shelf was largely

		Global Stage/Age (Ma)	Regional Stage	Onlap curve Lw Bw	Sea-level changes (m above PD) 100 0	Group	Local Term	
							NE King	SE King
Pennsylvanian	Upper	Gzhelian	Bursumian			Cisco	Strawn "A" limestone	Twin Peaks
			Virgilian					Anne Tandy
		303.7					Tandy shale	Tandy shale
		Kasimovian	Missourian			Canyon		Katz (5100) sandstone
		307.0						
	Middle	Moscovian	Desmoinesian			Strawn	Strawn "B" limestone	Strawn (5400) limestone
			Atokan			Atoka		Upper Smithwick /Strawn shale
	Lower	315.2					Caddo Limestone	
		Bashkirian	Morrowan			Morrow		Caddo Limestone

Figure 2. General stratigraphic chart in the study area. Local stratigraphic terms are modified from Gunn (1979) and Boring (1993). Onlap curve (third-order) and sea-level changes are adapted from Haq and Schutter (2008). The brown shading area shows the studied interval (unit). Lw = landward; Bw = basinward. Numerical ages for the global stages are from Gradstein and Ogg (2012).

blanketed with terrigenous clastic deposits fed by several discrete fluvial-deltaic systems (Fig. 1).

DATA AND METHODS

This study analyzed three cores of the Strawn limestone: Exxon 90 Bateman (~180 ft [55 m] in length) and Shell 2B Burnett (~16 ft [5 m] in length) in King County, and Sun 1A Mary B. Wallace (~67 ft [20 m] in length) in Kent County (Fig. 1). Forty core samples were taken for thin section preparation. These forty thin sections were stained with a mixed solution of Alizarin Red S and potassium ferricyanide solution to distinguish dolomite from calcite, and ferroan from nonferroan carbonate minerals, respectively (Dickson, 1966). Blue fluorescence epoxy was injected into rock samples in order to highlight pores and micropores when seen under a microscope.

Dunham's (1962) classification of limestone, with modifications by Embry and Klovan (1971), has been widely used to describe carbonate deposits. This classification system was developed to characterize textural properties that are most significant for interpreting depositional environments, specifically, the hydraulic energy level (Dunham, 1962; Lokier and Junaibi, 2016). Criteria used to classify platform carbonate deposits in Dunham's classification are the supporting fabric of the original sediment and the abundance of mud. However, Dunham's classification system is unsuitable for categorizing resedimented carbonates (i.e., gravity-/density-flow deposits). Currently, no satisfactory cataloging scheme exists for classifying carbonate density-flow deposits using a descriptive sedimentological approach. Therefore, we modified Dunham's classification to describe and classify both primary carbonates and carbonate density-flow deposits.

LITHOFACIES AND CYCLES

Lithofacies Description

In the studied cores, six major lithofacies are differentiated: (1) bioclast grainstones to mud-lean packstones (mud < 10%), (2) bioclast wackestones to mud-rich packstones (mud > 10%), (3) intraclast rudstones, (4) dark bioclast packstones to wackestones, (5) sandy bioclast packstones, and (6) black mudrocks. Detailed descriptions of these six lithofacies follow below.

Bioclast grainstones to mud-lean packstones are gray, and they show a massive structure or slightly normal grading in core samples. Under the microscope, this facies reveals abundant skeletal grains, of which echinoderm debris is the dominant element. Consistently associated with the echinoderms are bryozoans, small foraminifers, brachiopods, algae, mollusks, and ostracods (Figs. 3 and 4). Grains are between 0.1 and 2 mm in size. Grainstones to mud-lean packstones were observed in a few cored intervals in the Exxon 90 Bateman well (Fig. 4B).

Bioclast wackestones to mud-rich packstones are gray and massive, and some have a slight mottled fabric. Grains commonly comprise echinoderms, bryozoans, small foraminifers, phylloid algae, peloids, brachiopods, mollusks, ostracods, fusulinids, and trilobites (Fig. 5). Siliceous sponge spicules of various shapes are locally present. Calcite cements appear in some samples. This type of lithofacies is moderately present in the studied cores, and it may be highly porous (>10%).

Intraclast rudstones contain clasts that vary from very coarse sand to medium pebbles in size, and may be termed as intraclast conglomerates (Fig. 6). In slabbed cores, the intraclasts appear as tan to gray subangular clasts. Some intraclasts appear as semiopaque masses of cryptocrystalline calcareous mudstones or wackestones under a microscope. In addition to intraclasts, bioclasts may be present in a significant amount, including echinoderms and minor fusulinids, brachiopods and bryozoans. Intraclast rudstones commonly show poor sorting of grains, and may display reverse grading. The matrix may contain organic matters and probable clays. These grain-supported limestone conglomerates are commonly thinly to medium bedded and have sharp contacts with lower and upper beds, and they may be moderately inclined locally (Fig. 6B).

Dark bioclast packstones to wackestones are dark and very dense, and they show planar to wavy laminations or beddings (Fig. 7). Grains mainly include echinoderms, bryozoans, brachiopods, and other minor bioclasts. Crinoids are as much as 2.5 mm long, but most range between 0.2 and 1.5 mm. Brachiopods are as much as 5 mm in long axis. Typically, this lithofacies has sharp upper and lower contacts (Fig. 7A and 7B), and individual intervals vary from a few centimeters to a few decimeters and rarely are of meter-scale in thickness.

Sandy bioclast packstones are composed of mixed carbonates and siliciclastics (Fig. 8). Carbonate grains are mostly crinoids and bryozoans with minor amounts of brachiopods.
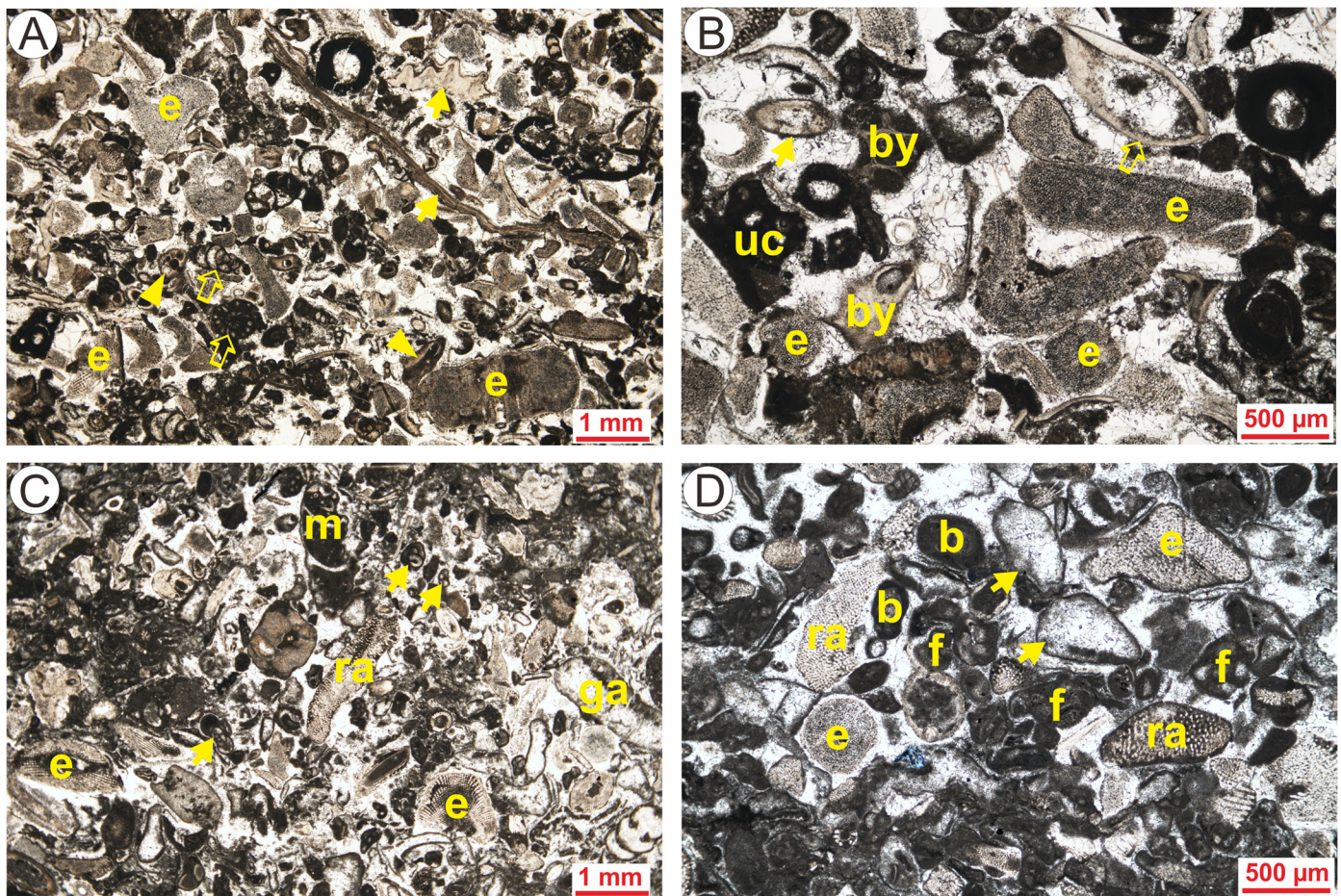
Figure 3. Photomicrographs showing bioclast grainstones and mud-lean packstones. (A) Bioclast grainstone. Echinoderms (e) are most common. Minor grains include foraminifers (hollow arrow), brachiopods (solid arrow), and bryozoans (triangle). Some bioclasts are unidentifiable; others are probably micritized fragments of bryozoans. Exxon 90 Bateman well, 5187.6 ft (1581.6 m) depth. (B) Bioclast grainstone. Major grains are echinoderms (e) and bryozoans (by), and minor grains include brachiopods (solid arrow) and ostracods (hollow arrow). Some unidentifiable grains (uc) are possibly micritized bryozoan fragments. Exxon 90 Bateman, 5187.6 ft (1581.6 m). (C) Bioclast mud-lean packstone. Echinoderms (e) and small foraminifers (solid arrow) are major grains. Mollusks (m) are relatively common. Both red algae (ra) and green algae (ga) are present. Mud matrix is locally present. Exxon 90 Bateman well, 5177.3 ft (1578.4 m). (D) Bioclast mud-lean packstone consists of mainly small foraminifers (f) and echinoderms (e). Minor bryozoans (b) and red algae (ra) are present. Some bioclasts are unidentifiable (arrow). Mud matrix is locally present. Exxon 90 Bateman, 5181.5 ft (1579.7 m).

Siliciclastic grains are dominantly quartz. Quartz grains are generally very fine in size, angular to subrounded in shape, and well sorted. Bioclasts vary from 0.5 to 1.5 mm in diameter. Glauconite is rarely observed (Fig. 8). This lithofacies contains dark, organic-rich stringers, and shows laminations or beddings in some cases. Soft-sediment deformation may be present. This lithofacies may be associated with dark (or black) mudrocks.

Black mudrocks contain a mixture of siliciclastic and carbonate muds. Concretions occur locally. Bioclasts may be sparsely present, including triangular bryozoan (*Prismopora triangulate*), fenestrate bryozoans, and some mollusks. Observable sedimentary structures are sparse and limited to occasional parallel laminations (Fig. 9). This lithofacies vary from nonfissile, to slightly fissile, or very fissile. Black mudrocks are interbedded with dark bioclast packstones to wackestones and occasionally with intraclast rudstones.

Cycles

Multiple scales of cycles are recognized in the Strawn limestone in King and Kent counties (Figs. 4 and 10). Meter-scale cycles commonly consist of a thin dark mudrocks (less than 2 ft [0.6 m]) succeeded by a relatively thick interval of bioclast wackestones to mud-rich packstones (commonly 5–20 ft [1.5–6.1 m]).

Several meter-scale cycles constitute a cycle set that reveals a large-scale trend. The lower part of some individual cycle sets in the studied cores is more dominated by black argillaceous mudrocks (2–30 ft [0.8–9 m] thickness), and commonly contains multiple intervals of density-flow deposits (e.g., intraclast rudstones and dark bioclast packstones to wackestones). The upper part is comprised of thick beds of bioclast wackestones to mud-rich packstones, and bioclast grainstones to mud-lean packstones intervals may exist in some cycle sets (Figs. 4B and 10).

Depositional Environments

Bioclast grainstones to mud-lean packstones are interpreted to have been deposited in a shallow-water setting of the inner ramp or on a paleotopographic high. Absence or scarcity of mud suggests a high-energy environment with turbulent waters and washout of much mud. The abundance and diversity of the biota (including crinoids, brachiopods, green algae, mollusks, bryozo-
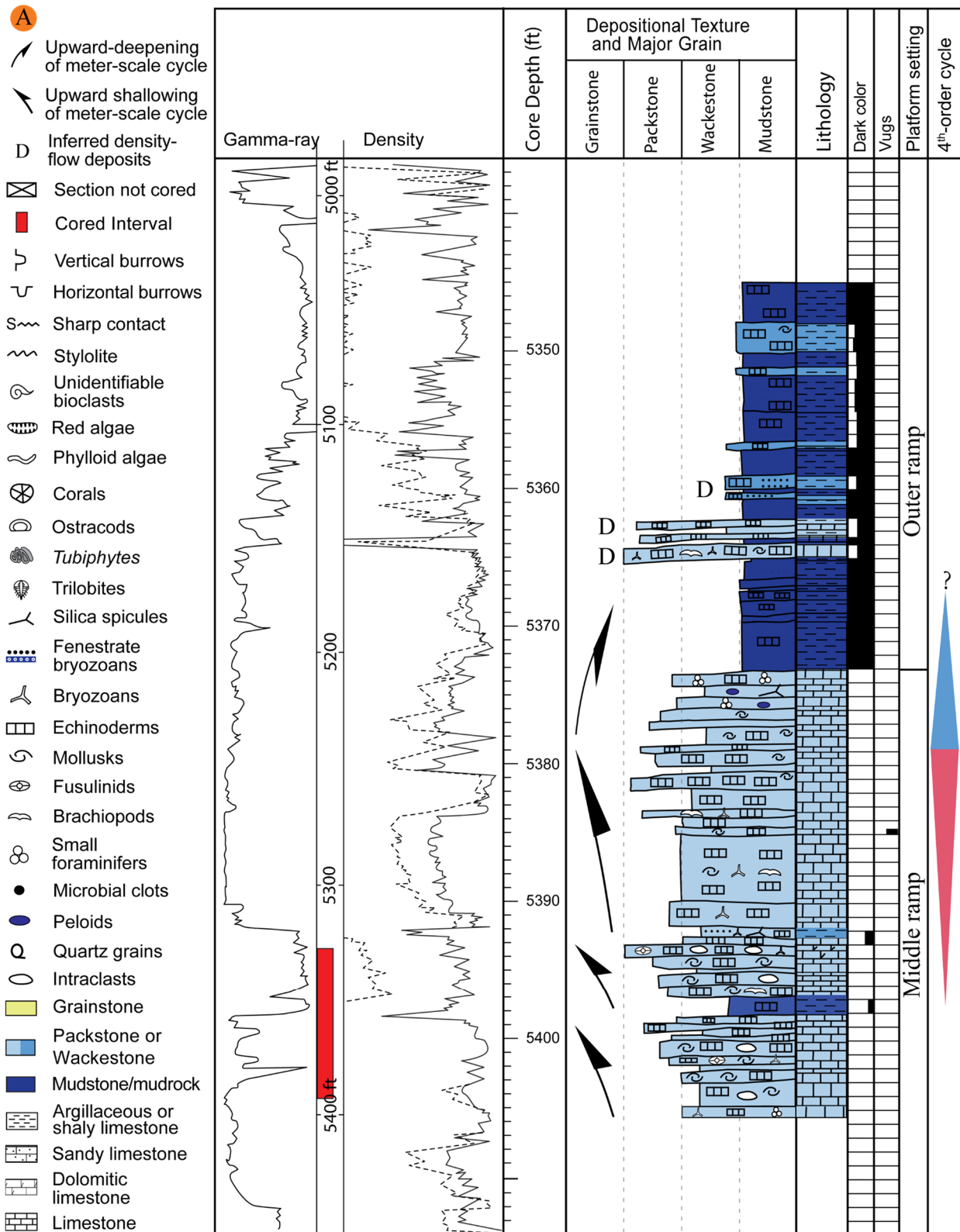
Figure 4. Stratigraphic column sections of the Exxon 90 Bateman well in King County, showing lithofacies with major grains, interpreted depositional environments, occurrence of vuggy pores, and some cycles on the basis of core and thin section observation. (A) Core depth: 5405–5345 ft (1647.9–1629.6 m). (B, see **Page 120**) Core depth: 5243–5165 ft (1598.5–1574.7 m). (C, see **Page 121**) Core depth: 5165–5120 ft (1574.7–1561.0 m).
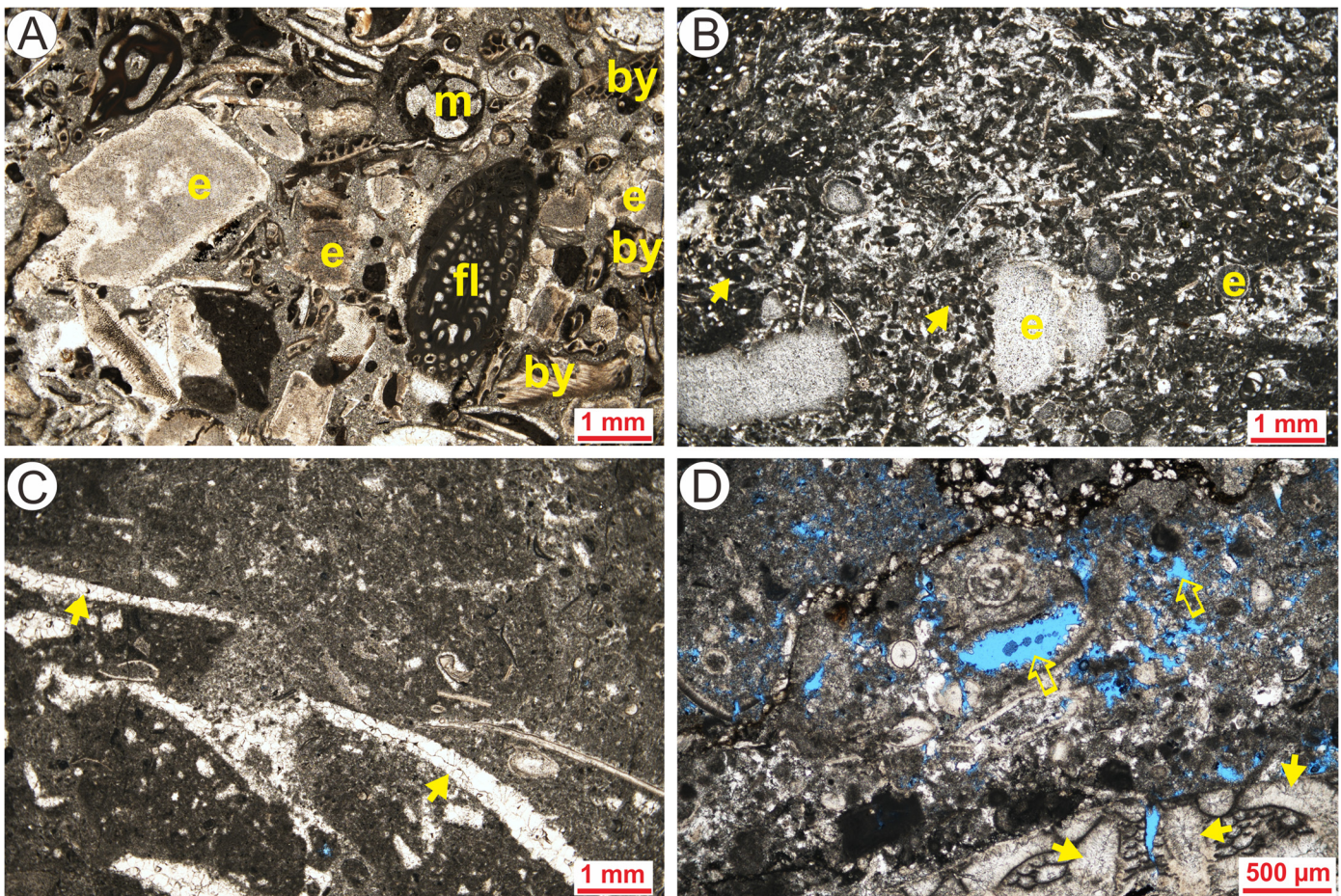
Figure 5. Photomicrographs showing bioclast wackestones and mud-rich packstones. (A) Mud-rich packstone contains a variety of grains. Echinoderms (e) are dominant. Subordinate grains include bryozoans (by), fusulinids (fl), mollusks (m), and other minor bioclasts. Shell 2B Burnett well, 5549.0 ft (1691.8 m) depth. (B) Mud-rich packstone contains abundant small foraminifers (arrow) and echinoderms (e). Exxon 90 Bateman, 5186.4 ft (1581.2 m). (C) Bioclast wackestone. Some bioclasts were probably phylloid algae or mollusks originally (arrow), but they dissolved and their molds were filled by calcite cement. Exxon 90 Bateman, 5404.5 ft (1648.0 m). (D) Bioclast wackestone. Note blade calcite cement (solid arrow) and open pores (hollow arrow). Exxon 90 Bateman, 5211.4 ft (1588.8 m).

ans, etc.) suggest deposition in a shallow-water marine environment of normal salinity (Yose and Heller, 1989).

Bioclast wackestones to mud-rich packstones were probably deposited in moderately-deep marine settings in the middle-ramp setting (commonly between fair-weather wave base and storm wave base), a well oxygenated, open-marine environment hospitable to a wide variety of marine fauna (Marquis and Laury, 1989; Flügel, 2004). The poor sorting and abundance of burrow-mottled matrix also suggest a low- to moderate-energy setting. This environment, however, might be subjected to episodic storm waves (Marquis and Laury, 1989).

Dark bioclast packstones to wackestones display sharp contacts (particularly the contacts with the underlying black mudrocks) (Fig. 7). They are interpreted as density-flow deposits that accumulated in outer-ramp environments. Their dark hue is believed to be mainly due to organic matter. Organic matter commonly occurs in reduced environments, e.g., outer ramp, deepwater basin floors, or restricted environments. Deposition of the density-flow packages signifies a large increase in the rate and volume of sediment supplied in the middle ramp or inner ramp, resulting in instability of unconsolidated or weakly consolidated bioclast sediments, either triggered by failure of rapidly deposited sediment or caused by an external trigger such as an earthquake or a storm (Yose and Heller, 1989).

Intraclast rudstone beds commonly show sharp contacts with the overlying and underlying strata, and the beds are moderately inclined locally (Fig. 6). This lithofacies is poorly sorted, and it contains abundant matrix with organic matter and probable clays, indicative of relatively deep water. Intraclasts show highly contrasted components (e.g., mud-lean packstone clasts vs. wackestone or mudrock clasts) suggestive of distinctly different depositional environments. All evidence suggests that intraclast rudstones are probably density-flow (debris-flow) sediments that redeposited in outer-ramp environments, generated by storms and strong wave action on the inner or middle ramp as slumps that transformed into debris flows downslope (Cook, 1977, Yose and Heller, 1989). Textural variations between clast-supported and matrix-supported deposits probably resulted from variations in distance of transport, the former having been transported relatively closer to the source (Krause and Oldershaw, 1979; Mullins et al., 1984).

Sandy bioclast packstones are associated with dark, argillaceous mud. It probably formed in moderate to relatively deep water settings. Glauconite is locally present, suggestive of relatively deep water (Marquis and Laury, 1989). Mixtures of quartz sands and bioclast grains were probably due to spatial variability. Mixing occurs mainly by lateral facies from coeval but varied sedimentary environments (Mount, 1984). On the King County
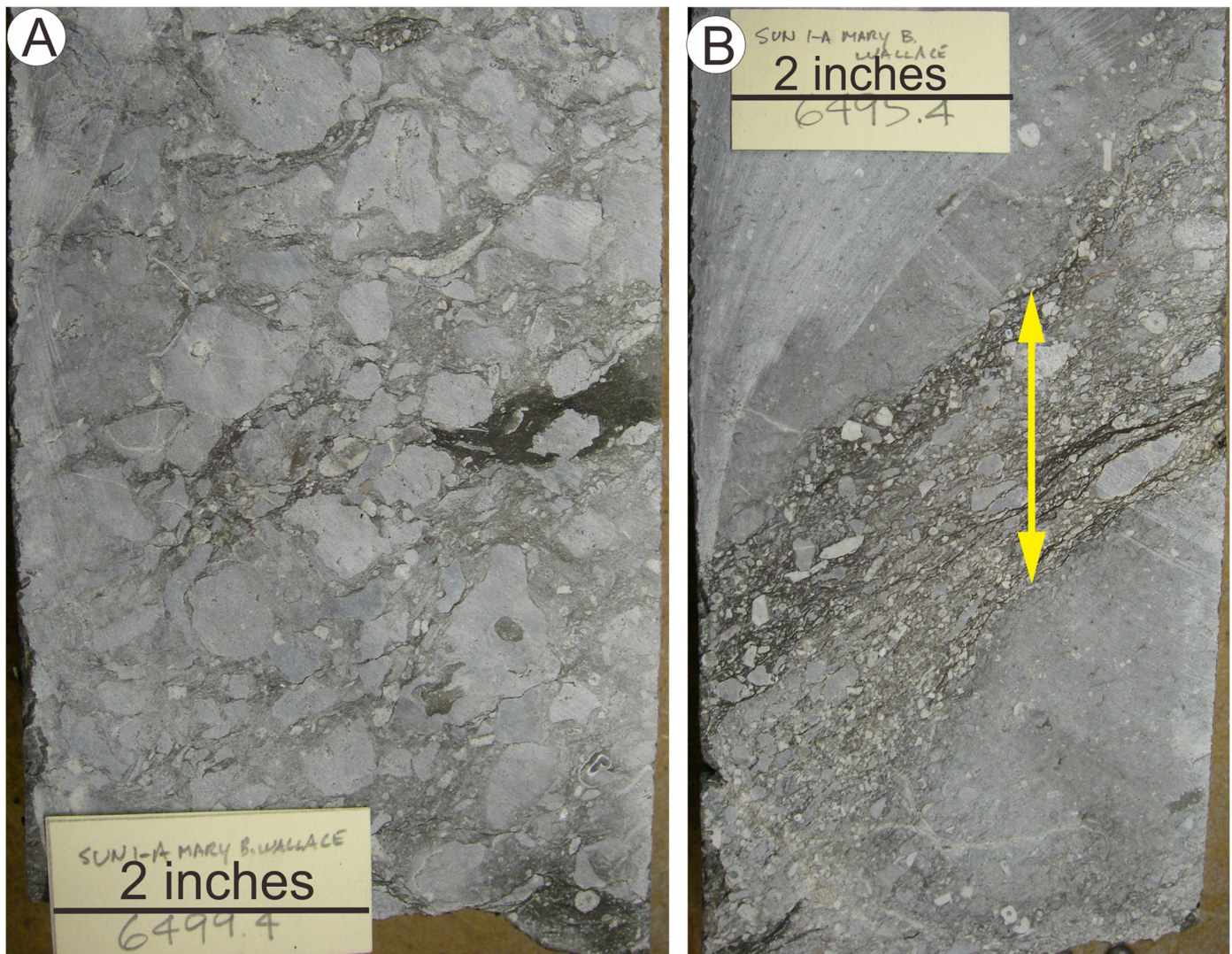
Figure 6. Photographs of slabbed cores showing intraclast rudstones. (A) Intraclast rudstone shows angular to subangular clasts. Sorting is poor. Sun 1A M. Wallace well, 6499.4 ft (1981.5 m) depth. (B) Inclined intraclast rudstone bed (arrow) showing the sharp upper and lower contacts. Sun 1A M. Wallace, 6495.4 ft (1980.3 m).

platform, the mixing of carbonate and siliciclastic sediments was attributed to progradation of the Haskell delta system along the Knox-Baylor Trough probably during sea-level falls and lowstands. Sporadic storms might transfer siliciclastic sediments from the delta systems to mixing with carbonates in the studied locations. Alternatively, mixing of siliciclastics and carbonates might have occurred along the diffuse boundaries between the two contrasting facies (Mount, 1984).

Black mudrocks display characteristics that support a deeper water (outer ramp) origin. The lack of algae, absence of burrows (bioturation), sparsity of the fauna, and local anoxic zones devoid of indigenous benthic fauna indicate a depositional environment having very low oxygen, and suggest a reducing, deepwater environment hostile to benthonic fauna (Gunn, 1979; Marquis and Laury, 1989).

In summary, bioclast grainstones to mud-lean packstones contain algal, foraminiferal, bryozoan, and echinoderm fragments, and they represent inner-ramp environments. Bioclastic wackestones to mud-rich packstones are interpreted to have been deposited in the middle ramp, an area having a moderate-energy environment and open-marine conditions hospitable to a wide variety of benthic fauna. The position and relatively greater thickness of the black mudrocks and the type and sparsity of the fauna suggest a poorly oxygenated type of depositional environment (the lower outer ramp). Density-flow sediments (intraclast rudstones, and dark bioclast packstones to wackestones) are commonly interbedded with black mudrocks; they accumulated in the outer-ramp environment.

Controls on Cyclicity

There has been controversies over third-order sequences in the Desmoinesian succession. Waite (1993) recognized a single sequence on the basis of seismic data across the Horseshoe Atoll area in the Midland Basin. Ross and Ross (1987, 1988) defined at least five third-order sequences (cycles) in north-central Texas. Our studied cores cover a small portions of the Strawn interval, and it is very difficult to analyze third-order cycles. However, numerous meter-scale cycles were identified in the Strawn limestone by the current study, which are the smallest stratigraphic cycles recognized in the cores, and most likely the fifth-order cycles (Kerans and Tinker, 1997). The cycle sets are bundles of cycles that display a consistent trend in cycle (or facies) stacking pattern, and probably represent the fourth-order cycles.

Figure 7. Core photographs (A and B) and photomicrographs (C and D) showing dark bioclast packstones and wackestones. (A) Dark bioclast packstone (bp) displays sharp lower contact with black mudstone (ms). Note that the subtle laminations in the underlying mudstone are truncated by scour surface (arrow). Exxon 90 Bateman well, 5211.4 ft (1588.9 m) depth. (B) Dark bioclast wackestone (bw) and packstone (bp) showing sharp contacts with underlying and overlying mudstone, respectively (arrow). Exxon 90 Bateman, 5137 ft (1566.2 m). (C) Dark bioclast packstone consists of dominant echinoderms and other minor skeletal fragments. Exxon 90 Bateman, 5145.7 ft (1568.8 m). (D) Dark bioclast wackestone. Echinoderms (e) and bryozoans (arrow) are sparsely to moderately present. Exxon 90 Bateman, 5139.2 ft (1566.8 m).
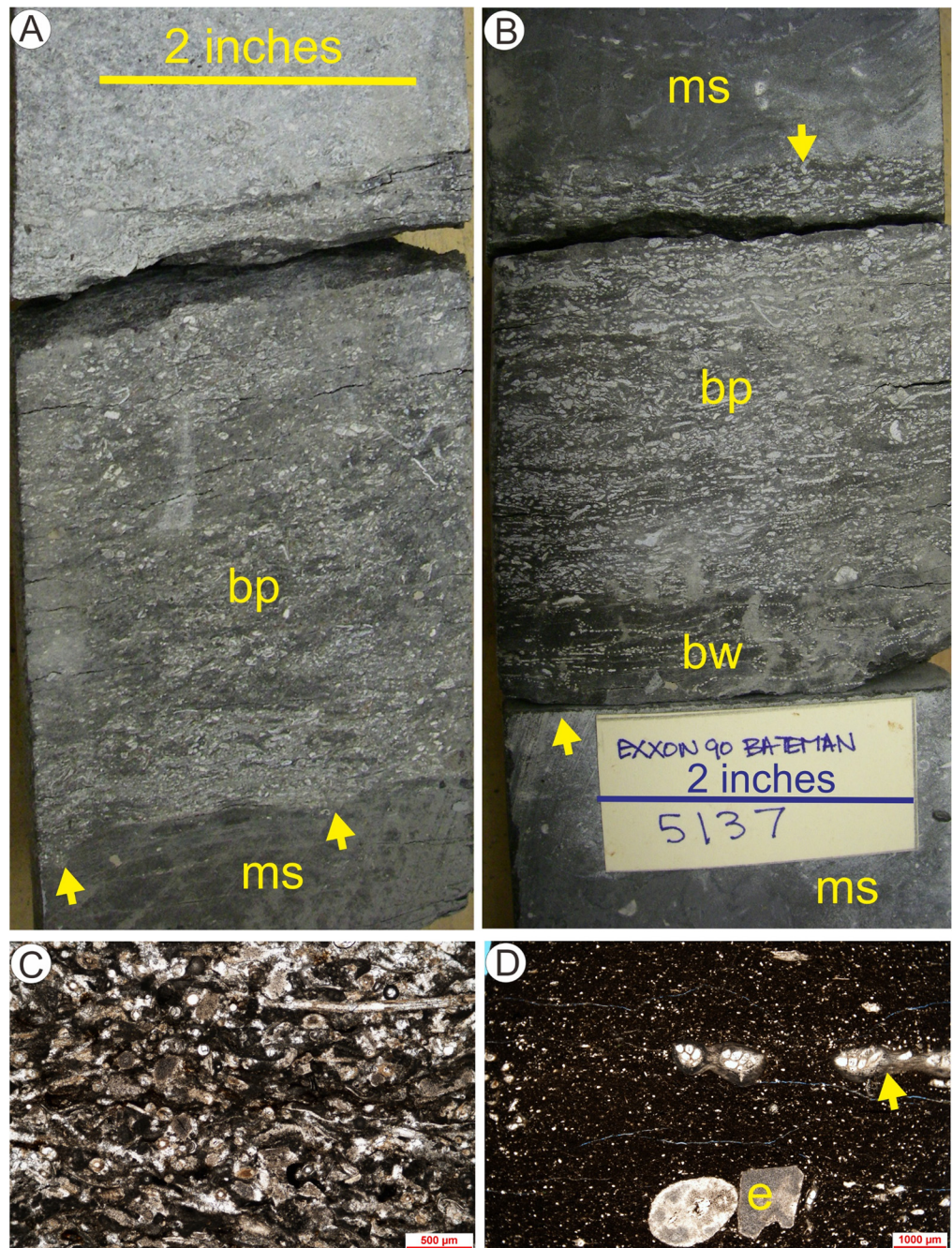
In the Exxon 90 Bateman and Sun 1A Mary B. Wallace wells, the cyclic deposits show periodic upward shoaling, signifying that the depositional environments shifted significantly as relative sea level changed. During the late-stage transgression and earliest high stands of sea level, an outer-ramp environment dominated the north edge of the Knox-Baylor Trough, in which black mudrocks and density-flow deposits accumulated. Whereas during lowstands (including late regression) of sea-level, the studied locations shifted to an inner-ramp setting, and bioclast grainstones to mud-lean packstones were deposited. During the transition intervals between the lowstand and highstand (e.g., early transgression), the locations changed to a middle-ramp environment, and bioclast wackestones to mud-rich packstones deposited. The frequent sea-level changes and resultant periodic shifts of depositional environments led to deposition of cyclic sediments.

Glacio-eustatic sea level fluctuations were thought to be the dominant control on the observed cyclicity and facies distribution (Heckel, 1986, 2008; Marquis and Laury, 1989). Local subsidence and delta progradation possibly added lesser modifications. The lithofacies asymmetry of cyclothems in the Strawn limestone (thinner transgressive units overlain by thicker regressive facies) supports the interpretation of glacio-eustatic sea-level variations as a dominant factor. Lithofacies asymmetry has been demonstrated to reflect rapid transgressions and slow regressions controlled by glacio-eustatic changes (Boardman et al., 1984; Heckel, 1986; Marquis and Laury, 1989). Glacio-eustatic sea level changes have been reported as the causal mechanism of the cyclicity in the Strawn Desmoinesian strata in Texas, the Mid-Continent, and other places (Cleaves, 2000; Wright, 2011).
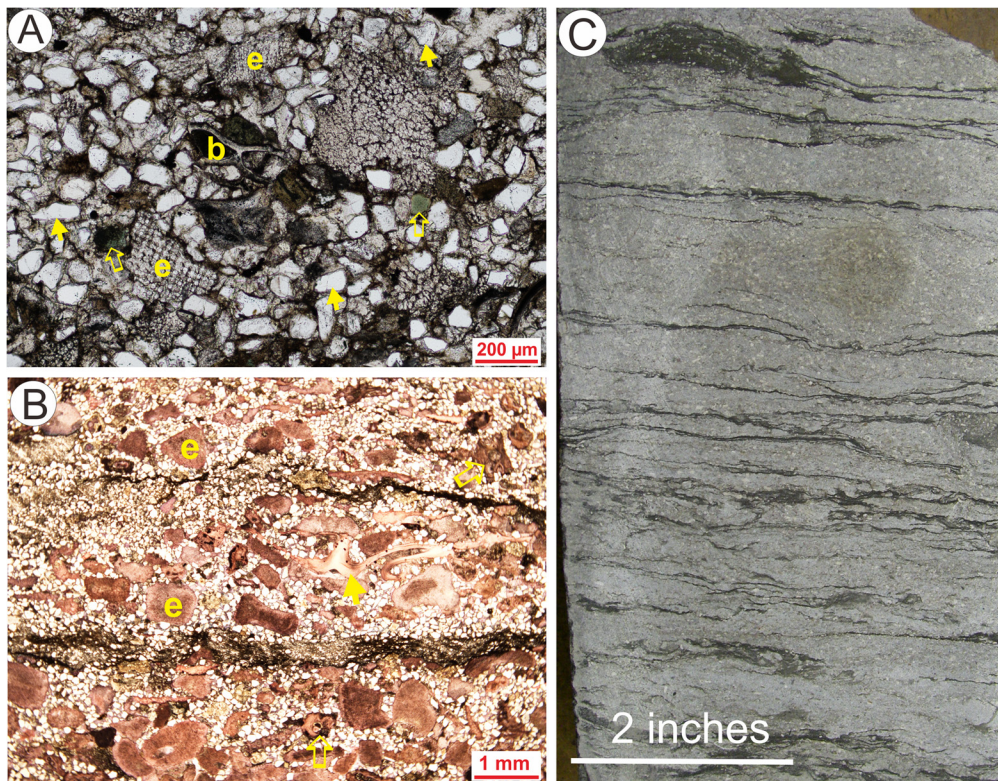
Figure 8. Photomicrographs (A and B) and core image (C) showing sandy bioclast packstones. (A) Sandy bioclast packstone contains common grains: echinoderms (e), bryozoans (b), and quartz (arrows). Note that glauconite is present (hollow arrows). Exxon 90 Bateman well, 5151.7 ft (1570.6 m) depth. (B) Sandy bioclast packstone. Dominant grains are echinoderms (e), and minor bioclasts include bryozoans (hollow arrow) and brachiopods (solid arrow). Quartz grains (in white color) are abundant. Bioclasts have been stained in red by Alizarin Red S. Sun 1A M. Wallace, 6491.0 ft (1979.0 m). (C) Sandy bioclast packstone showing irregular laminations or very thin beddings. Note dark stringers (probably clayey stringers). Sun 1A M. Wallace, 6491.8 ft (1979.2 m).

MAJOR DIAGENETIC FEATURES AND INTERPRETATION

Cementation

Four types of carbonate cements are observed in the Strawn limestone: blade calcite cement, syntaxial-overgrowth calcite cement, drusy mosaic calcite cement, and saddle dolomite cement.

Blade calcite cement fringes grains, and fill intragranular pores (especially chambers of fusulinids), forming rims about 100 µm thick (Figs. 5D and 11A). Blade calcite cement is the first generation of cement in the Strawn limestone.

Blade calcite cement formed in seawater or in marine phreatic environments. It possibly precipitated as aragonite but it subsequently neomorphosed to calcite (James and Choquette, 1990; Flügel, 2004).

Syntaxial calcite cement appears as overgrowths on echinoderm fragments (grains), and it shows optical continuity with a grain such that the original crystal and the overgrowth form a single larger crystal. Some overgrowth cement displays a compromised planar boundary with adjacent overgrowth cement, forming a polygonal suture pattern (Fig. 11B).

Syntaxial overgrowths occur in marine, meteoric, and burial diagenetic settings (Scholle and Ulmer-Scholle, 2003). In the Strawn limestone, syntaxial overgrowths are extensive in bioclast limestones that show no evidence of meteoric diagenesis, which argues against precipitation in meteoric environments. A polygonal suture pattern of overgrowth cement seems to be characteristic of shallow-marine cements (Moore and Wade, 2013).

Drusy mosaic calcite crystals increase in size from the edges toward the center of the antecedent pores. They are commonly very fine to finely crystalline, and they show planar-anhedral crystal boundaries (Figs. 11C and 11D). This type of cement is observed mostly in bioclast wackestones to mud-rich packstones as well as grainstones to mud-lean packstones.

Drusy mosaic calcite cement is generally thought to be a burial cement, although it can also form in meteoric environments (Scholle and Ulmer-Scholle, 2003). Drusy mosaics in the studied samples fill dissolution vugs and molds, which suggests that they might postdate meteoric diagenesis and probably have formed in burial environments.

Saddle dolomite cement are readily recognizable because they have curved crystal faces (Figs. 11E and 11F). In the Strawn limestone, some crystals show undulose extinction. The cement crystals vary from fine to medium crystalline in size (mostly < 300 µm), shows opaque white color, and are commonly subhedral. Compared with typical saddle dolomite that coarsely to extremely coarsely crystalline (Qing and Mountjoy, 1994; Spötl and Pitman, 1998), the Strawn saddle dolomite is much finer in crystal size. This type of cement seems to the latest stage, and commonly lines or fills vugs and molds.

Saddle dolomite commonly forms at elevated temperatures and in association with hydrothermal fluid events (Radke and Mathis, 1980; Davies and Smith, 2006). In the Strawn limestone, saddle dolomite postdates all cements and is believe to precipitate in relatively late burial stage.

Dissolution

Vugs and molds are abundant in thick packstone to wackestone intervals in the Exxon 90 Bateman and Shell 2B Burnett wells, and not observed in the samples from the Sun 1A Mary B well (Figs. 11F and 12). In the Exxon 90 Bateman well, abundant vugs occur a wackestone to packstone interval having ~30 ft (9 m) thickness. Most vugs are irregularly shaped, and they vary in size from tens of microns to as much as 0.4 in (1 cm). Molds display a variety of shapes, commonly resembling former individual constituents of the sediment or rock. Some molds are very elongate, whereas others are roughly rounded or oval (Fig. 12B).

Vugs are not fabric selective. In other words, vugs do not specifically conform in shape or boundary to particular fabric elements of the host rock, and they result from nonselective dis-

Figure 9. Core photographs of dark/black mudrocks. (A) Slightly fissile mudrock with rare bioclasts. Exxon 90 Bateman well, 5131.3 ft (1564.4 m) depth. (B) Black mudrock is fissile. Exxon 90 Bateman, 5368.5 ft (1636.7 m).
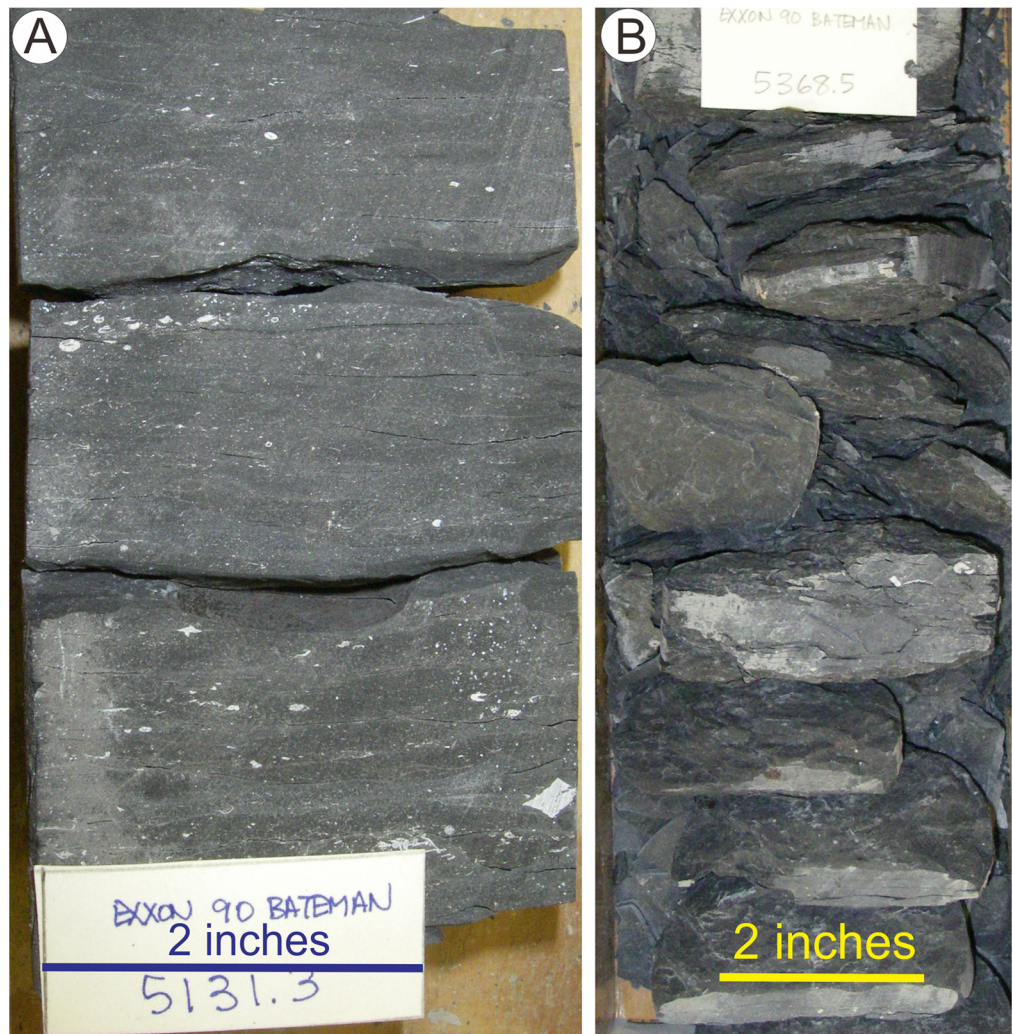
solution (Choquette and Pray, 1970). Molds in sedimentary carbonates form by the selective dissolution of various types of carbonate grains (Scholle and Ulmer-Scholle, 2003). In Strawn limestone, the periphery of many molds appears to mimic the outline of molluscan shells, phylloid algae, and small foraminifers, although it is often challenging to identify initial constituents of molds (Figs. 11F and 12). Generally, the micrite envelopes and the outlines of molds are the only remaining evidence of original algal blades, molluscan shells, and foraminiferal casts. Other molds might result from leaching of bryozoans or unidentifiable bioclasts. The unstable allochems were largely composed of aragonite or high–Mg calcite, and therefore they were preferentially partially to completely leached out, or neomorphosed to calcite (Moshier and Kirkland, 1993; Saller et al., 1994; Wahlman, 2002; Fu et al., 2017).

Formation of vugs and molds in the Strawn limestone is related to meteoric diagenesis during sea-level lowstands, when the inner ramp and possibly parts of the middle ramp were subaerially exposed (Marquis and Laury, 1989; Cleaves, 2000). In the studied samples, the greatest dissolution generally occurred in the bioclast wackestones and packstones containing aragonitic and high–Mg components. In some cases, leaching of matrix also occurred, which created micro-vugs or enhanced matrix pores. Echinoderm fragments show little or no evidence of dissolution effects. Intergranular pores were not observed in the grainstones and mud-lean packstones, likely because early cementation occluded pore spaces.

PORE TYPES AND CONTROL FACTORS

In the studied cores of the Strawn limestone in King and Kent counties, various pore types exist: interparticle (intergranular and intercrystalline), intragranular, vugs, molds, and dissolution-enhanced matrix pores (Figs. 12 and 13). Among these, vugs and molds are the dominant pores (Figs. 11F and 12).

Intergranular pores generally vary from 10 to 200 μm in size (Fig 13A). They are primary but may be enhanced by dissolution. Intergranular pores are uncommon; when present they occur mainly in the bioclast mud-rich packstones. In the grainstone and mud-lean packstone intergranular pores are largely occluded by cements. Intragranular pores are sparse and mostly restricted within fusulinids and minor bryozoans (Fig. 13B). Intercrystalline pore sizes range between 100 and 500 μm, and these pores are commonly associated with replacement and cement dolomite crystals (Fig. 13C). Enhanced matrix pores (or micro-vugs, < 60 μ) are present in moderate amounts (Fig. 13D) in the relatively porous samples.

In the studied cores, significant (reservoir-quality) pores are only seen in a specific lithofacies: bioclast wackestones to mud-rich packstones. They are absent from other lithofacies. Secondary vugs and molds are the major type of pores, and total porosity is mainly controlled by the intensity of meteoric dissolution and the distribution of marine and burial cement.

The Strawn bioclast grainstones to mud-lean packstones in the study area are interpreted to have been deposited in the inner
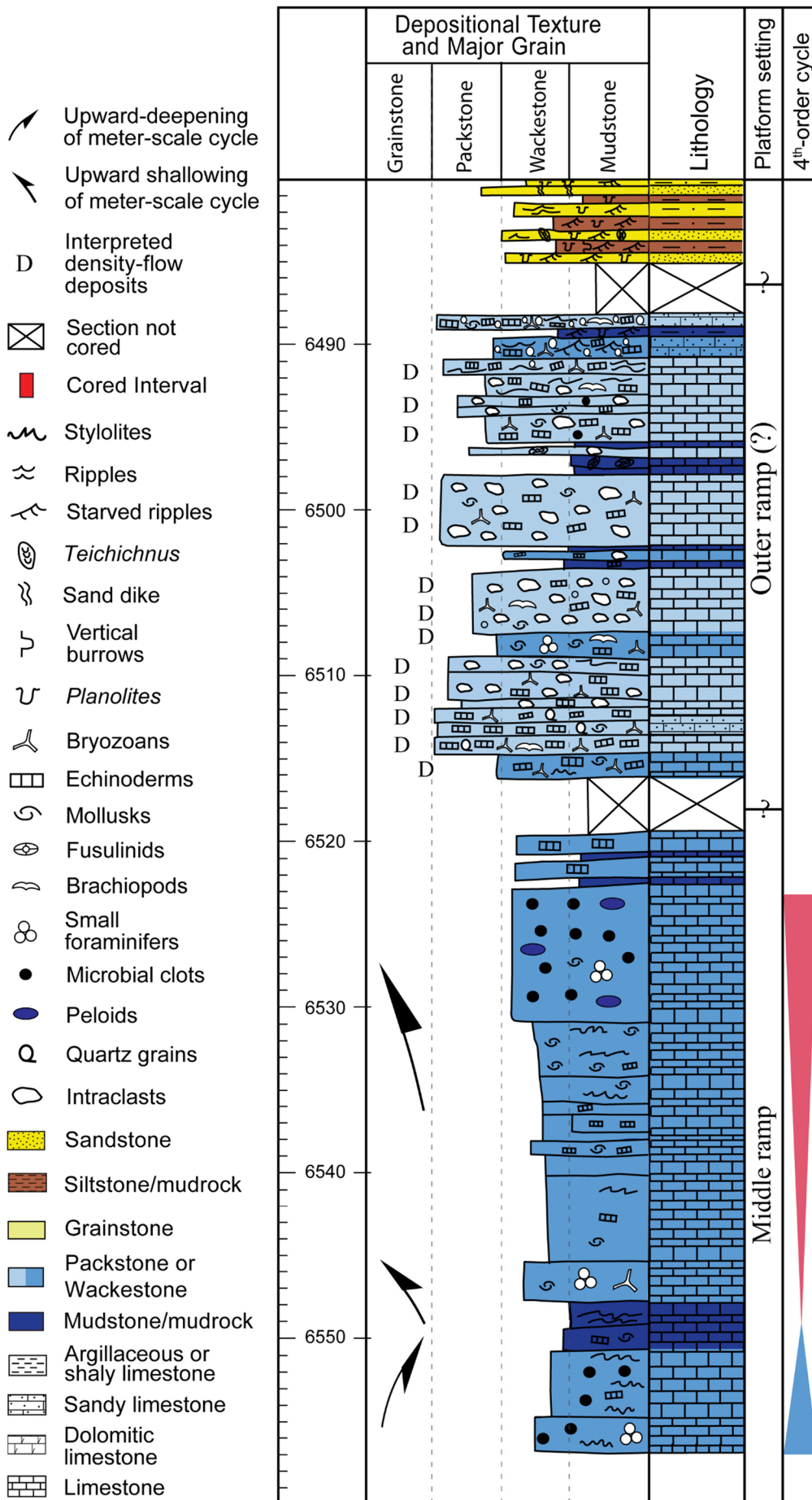
Figure 10. Stratigraphic column section showing lithofacies with major grains, interpreted depositional environments, and some cycles on the basis of core and thin section observation. Sun 1A M. Wallace well in Kent County.
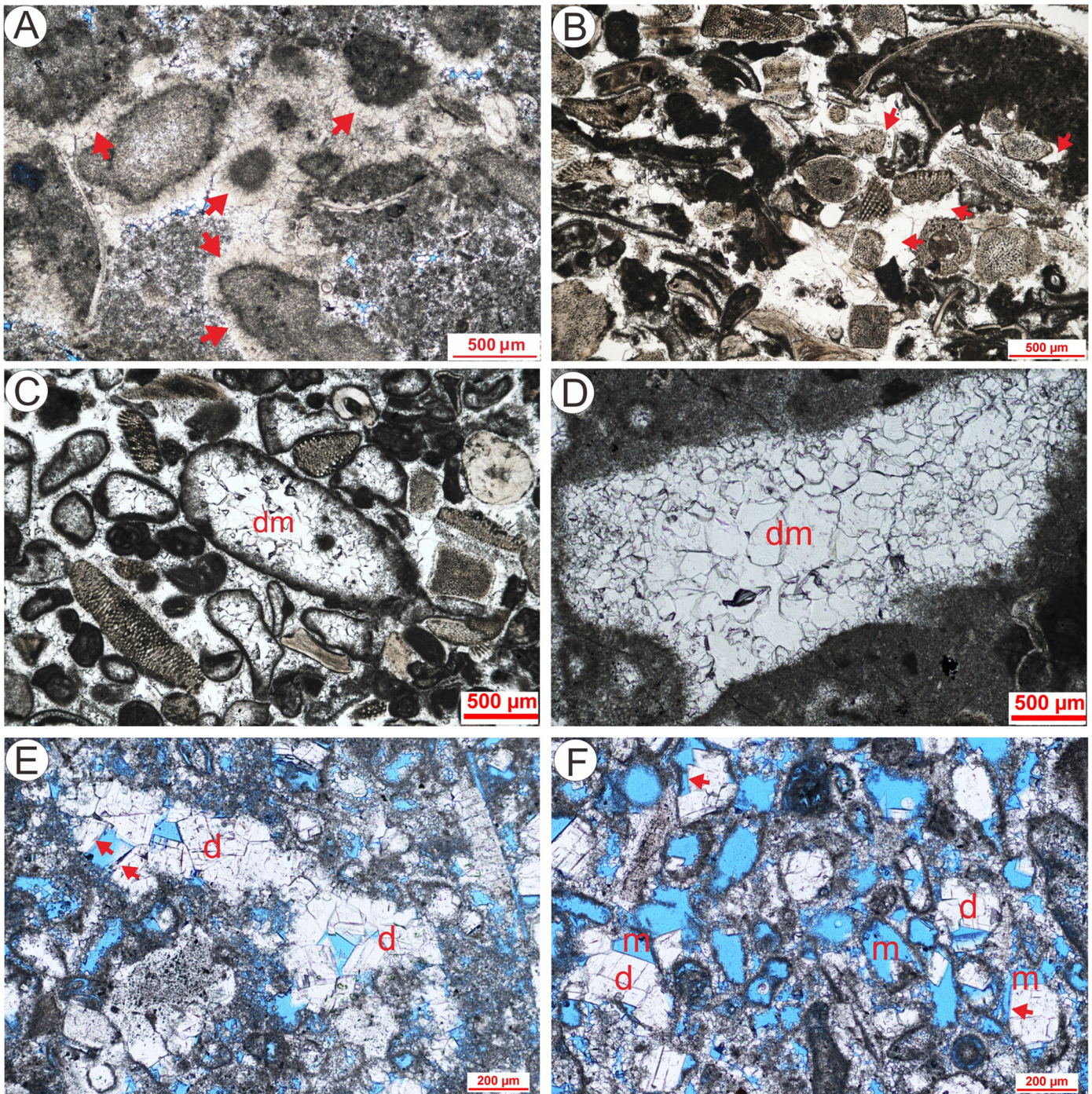
Figure 11. Photomicrographs showing a variety of cements in the Strawn limestone. **(A)** Blade calcite cements (arrow) fringing neomorphised grains. **Exxon 90 Bateman well, 5215.9 ft (1590.2 m) depth. (B)** Syntaxial calcite cement (arrow) overgrowths on echinoderms. **Exxon 90 Bateman, 5187.6 ft (1581.6 m). (C)** Drusy mosaic calcite cement (dm). **Exxon 90 Bateman, 5181.5 ft (1579.7 m). (D)** Drusy mosaic calcite cement (dm). **Exxon 90 Bateman, 5393.2 ft (1644.2 m). (E)** Saddle dolomite cement (d) partly occludes vugs. **Note curved crystal faces (arrow). Shell 2B Burnett, 5557.0 ft (1694.2 m). (F)** Saddle dolomite cement (d) partly occludes molds (m). **Note curved crystal surface (arrow). Shell 2B Burnett, 5557.0 ft (1694.2 m).**

ramp, and reveal no visible open pores under microscope (Fig. 3). The sediments in sea floor contains normal or modified marine pore fluids that are commonly supersaturated with respect to most types of carbonate minerals, and pores are potentially the sites of extensive marine cement precipitation (Tucker and Wright, 1990; Moore and Wade, 2013). Marine cementation is largely controlled by the rate of fluid movement through the sediment pore system and hence is greatly affected by energy condi-

tions at the site of deposition as well as by sediment porosity and permeability (Moore and Wade, 2013). In other words, cementation is favored in high-energy settings where sediments are both originally porous and permeable (because of the lack or scarcity of mud) and where rates of water flux and CO_2 degassing are high. The Strawn bioclast grainstones to mud-lean packstones are inferred to have been deposited in the inner ramp with strong wave or current agitation. They probably had been extensively
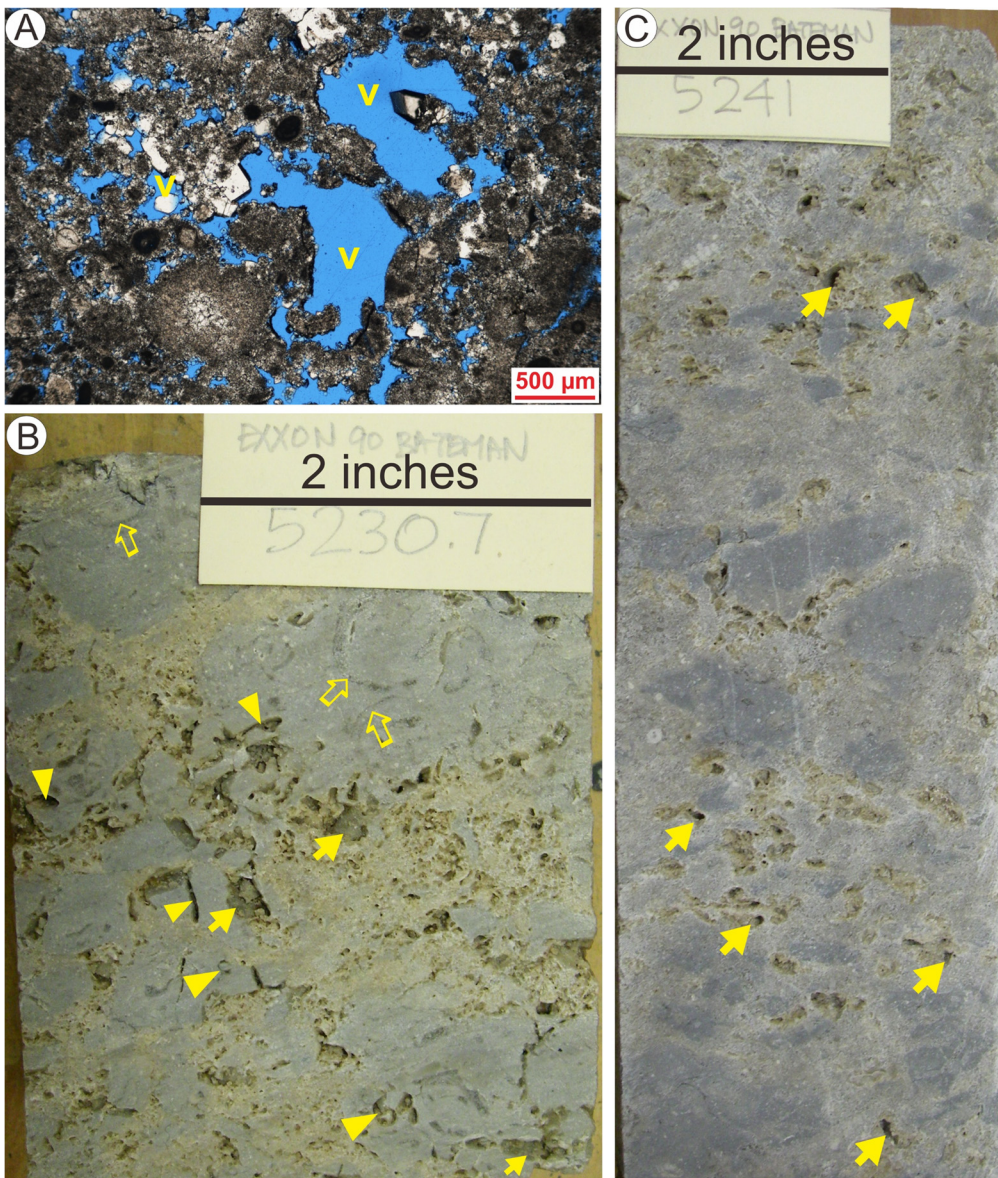
Figure 12. Dissolution vugs and molds. (A) Photomicrograph showing abundant vugs (v). Exxon 90 Bateman well, 5215.9 ft (1590.2 m) depth. (B) Core photograph showing abundant vugs (solid arrow) and molds (triangles). Note possible phylloid algae plates (hollow arrow). Exxon 90 Bateman, 5230.7 ft (1594.7 m). (C) Core photograph showing vugs (arrow). Exxon 90 Bateman, 5241.0 ft (1597.9 m).

cemented (e.g., by blade and syntaxial overgrowth cement) and become very tight before meteoric diagenesis. Therefore, the fresh water could not have penetrated and leached the lithofacies to create dissolution pores.

The Strawn bioclast wackestones to mud-rich packstones contain extensive secondary pores. Vugs and molds are associated with neomorphic calcite in many cases, suggesting a meteoric-dissolution origin (Scholle and Ulmer-Scholle, 2003). The distribution of secondary pores (vugs and molds) conforms to bioclast wackestones to mud-rich packstones in the upper unit of individual cycle sets (i.e., fourth-order cycles; Figs. 4B and 10), suggesting that meteoric leaching occurred as a result of near-surface freshwater lenses that migrated to the middle ramp primarily in response to fourth-order sea-level falls. Thus, the upper regressive parts of individual stratigraphic cycle sets may be highly porous, which contrasts sharply with the unaltered nonporous transgressive portions.

The dominant porosity-reducing processes included early cementation in near-surface settings, compaction, and burial environments (especially late-stage saddle dolomite cementation in a deeper burial environment).

SUMMARY AND CONCLUSIONS

In the studied cores of Strawn limestone, six major lithofacies were identified. Bioclast grainstones to mud-lean packstones are interpreted to have been deposited in the inner-ramp, bioclast wackestones to mud-rich packstones in the middle-ramp, and black mudrocks in the outer-ramp environments. Intraclast rudstones and dark packstones to wackestones are inferred to be density-flow deposits that accumulated in the outer-ramp setting. Sandy bioclast packstones might result from lateral facies mixing of coeval but varied sedimentary environments.

Meter-scale cycles and fourth-order cycle sets were recognized in the studied Strawn limestone. The lower part of a cycle or cycle set commonly comprises dark or black mudrocks, representing transgressive unit deposited in an outer-ramp setting with relatively deep water; the upper part consists of bioclast wackestones to mud-rich packstones plus bioclast grainstones to mud-lean packstones in some cycle sets, signifying the middle- to inner-ramp environments. Relative sea-level changes are the most viable mechanism for explaining the lithofacies associations and variations in the studied cores.
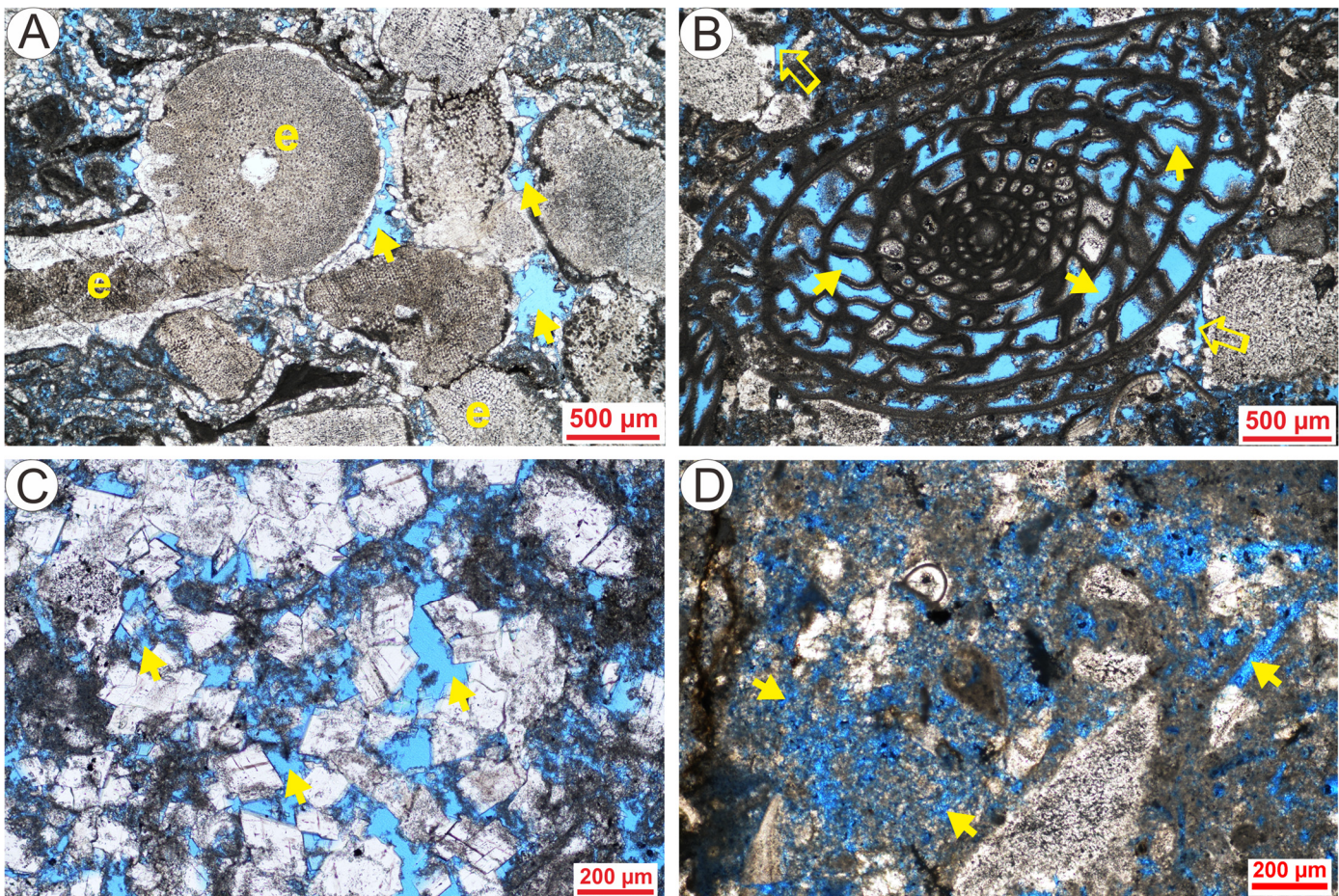
Figure 13. Photomicrographs showing various pores. (A) Intergranular pores (arrow) lined by calcite cement. Echinoderms (e) are major grains. Shell 2B Burnett well, 5553.0 ft (1693.0 m) depth. (B) Intragranular pores (arrow) within fusulinids, and minor intergranular pores (hollow arrow). Shell 2B Burnett, 5329.0 ft (1624.7 m). (C) Intercrystalline pores (arrow). Shell 2B Burnett, 5557.0 ft (1694.2 m). (D) Enhanced matrix pores (arrow). Sun 1A M. Wallace, 6512.5 ft (1985.5 m).

The Strawn carbonate reservoirs in the study area are highly heterogeneous. Vugs and molds are dominant pores, and other subordinate voids include intercrystalline, intergranular, intragranular, and dissolution-enhanced matrix pores. Porous zones generally conform to bioclast wackestones to mud-rich packstones facies in the upper unit of individual cycle sets. The major secondary-pore forming process in the Strawn limestone was early meteoric dissolution related to freshwater lenses that migrated in response to glacio-eustatic sea level changes.

ACKNOWLEDGMENTS

REFERENCES CITED

Boardman, D. R., R. H. Mapes, T. E. Yancey, and J. M. Malinky, 1984, A new model for the depth-related allogenic community succession within North American Pennsylvanian cyclothems and implications on the black shale problem, *in* N. J. Hyne, ed., Limestones of the Mid-Continent: Tulsa Geological Society Special Publication 2, Oklahoma, p. 141–182.

Boring, T. H., 1993, Upper Strawn (Desmoinesian) carbonate and clastic depositional environments, southeast King County, Texas, *in* K. S. Johnson and J. A. Campbell, J. A., eds., Petroleum-reservoir geology in the southern Midcontinent, 1991 symposium: University of Oklahoma, Norman, p. 195–198.

Choquette, P. W., and L. C. Pray, 1970, Geologic nomenclature and classification of porosity in sedimentary carbonates: American Association of Petroleum Geologists Bulletin, v. 54, p. 207–250.

Cleaves, A. W., 1993, Sequence stratigraphy, systems tracts, and mapping strategies for the subsurface Middle and Upper Pennsylvanian of the eastern shelf, *in* R. E. Crick, ed., American Association of Petroleum Geologists Southwest Section Meeting Transactions: Fort Worth Geological Society, Texas, p. 26–42.

Cleaves, A. W., 2000, Sequence stratigraphy and reciprocal sedimentation in Middle and Late Pennsylvanian carbonate-bank systems, eastern shelf of the Midland Basin, north-central Texas, *in* K. S. Johnson, ed., Platform carbonates in the southern Midcontinent: University of Oklahoma, v. 101, p. 227–257.

Cleaves, A. W., and A. W. Erxleben, 1985, Upper Strawn and Canyon cratonic deposition of the Bend Arch, north-central Texas, *in* C. L. McNulty and J. C. McPherson, eds., American Association of Petroleum Geologists Southwest Section Meeting Transactions: Fort Worth Geological Society, Texas, p. 27–46.

Cook, H. E., 1977, Ancient continental slopes and their value in understanding modern slope development, *in* L. J. Doyle and O. H. Pilkey, eds., Geology of continental slopes: Society of Economic Paleontologists and Mineralogists Special Publication 27, Tulsa, Oklahoma, p. 287–305.

Davies, G. R., and L. B. Smith Jr., 2006, Structural controlled hydrothermal dolomite reservoir facies: An overview: American Association of Petroleum Geologists Bulletin, v. 90, p. 1641–1690.

Dickson, J. A. D., 1966, Carbonate identification and genesis as revealed by staining: Journal of Sedimentary Petrology, v. 36, p. 491–505.

Dunham, R. J., 1962, Classification of carbonate rocks according to depositional textures, *in* W. E. Ham and L. C. Pray, eds., Classification of carbonate rocks—A symposium: American Association of Petroleum Geologists Memoir 1, Tulsa, Oklahoma, p. 108–121.

Embry, A. F., and J. E. Klovan, 1971, A Late Devonian reef tract on northeastern Banks Island, NWT: Bulletin of Canadian Petroleum Geology, v. 19, p. 730–781.

Flügel, E., 2004, Microfacies of carbonate rocks: Analysis, interpretation and application: Springer, Berlin, Germany, 976 p.

Fu, Q., W. A. Ambrose, and J. W. Barton, 2017, Reservoir characterization of the Pennsylvanian Caddo Limestone in Stephens County, Texas: A case study of *Komia*-dominated algal mounds: Marine and Petroleum Geology, v. 86, p. 991–1013.

Gradstein, F. M., and J. G. Ogg, 2012, The chronostratigraphic scale, *in* F. M. Gradstein, J. G. Ogg, M. D. Schmitz, and G. M. Ogg, eds., The geologic time scale: Elsevier, Amsterdam, The Netherlands, p. 31–42.

Gunn, R. D., 1979, Desmoinesian depositional systems in the Knox-Baylor Trough, *in* N. J. Hyne, ed., Pennsylvanian sandstones of the Mid-Continent: Tulsa Geological Society, Oklahoma, p. 221–234.

Haq, B. U., and S. R. Schutter, 2008, A chronology of Paleozoic sea-level changes: Science, v. 322, p. 64–68.

Heckel, P. H., 1986, Sea-level curve for Pennsylvanian eustatic marine transgressive-regressive depositional cycles along Midcontinent outcrop belt: North America: Geology, v. 14, p. 330–334.

Heckel, P. H., 1995, Glacial-eustatic base-level–climatic model for late Middle to Late Pennsylvanian coal-bed formation in the Appalachian Basin: Journal of Sedimentary Research, v. B65, p. 348–356.

Heckel, P. H., 2008, Pennsylvanian cyclothems in Midcontinent North America as far-field effects of waxing and waning of Gondwana ice sheets, *in* C. R. Fielding, T. D. Frank, and J. L. Isbell, eds., Resolving the Late Paleozoic ice age in time and space: Geological Society of America Special Paper 441, Boulder, Colorado, p. 275–289.

Hills, J. M., 1984, Sedimentation, tectonism, and hydrocarbon generation in Delaware Basin, West Texas and southeastern New Mexico: American Association of Petroleum Geologists Bulletin, v. 68, p. 250–267.

James, N. P., and P. W. Choquette, 1990, Limestones: The sea-floor diagenetic environment, *in* I. A. Mcllreath and D. W. Morrow, eds., Diagenesis: Geoscience Canada Reprint Series, v. 4, p. 13–34.

Krause, F. F., and A. E. Oldershaw, 1979, Submarine carbonate breccia beds—A depositional model for two-layer sediment gravity flows from the Sekwi Formation (Lower Cambrian), Mackenzie Mountains, Northwest Territories, Canada: Canadian Journal of Earth Sciences, v. 16, p. 189–199.

Lee, P., 2019, Burnett Ranch: A CO_2 flood on the Eastern Shelf of the Permian Basin, King County, Texas: American Association of Petroleum Geologists Search and Discovery Article 11234, Tulsa, Oklahoma, 1 p., <http://www.searchanddiscovery.com/abstracts/html/2019/dallas-90343/abstracts/2019.PS.40.html>.

Lokier, S. W., and M. A. Junaibi, 2016, The petrographic description of carbonate facies: Are we all speaking the same language?: Sedimentology, v. 63, p. 1843–1885.

Marquis, S. A., and R. L. Laury, 1989, Glacio-eustasy, depositional environments, diagenesis, and reservoir character of Goen Limestone cyclothem (Desmoinesian), Concho Platform, Central Texas: American Association of Petroleum Geologists Bulletin, v. 73, p. 166–181.

Moore, C., and W. J. Wade, 2013, Carbonate reservoirs, porosity and diagenesis in a sequence stratigraphic framework: Elsevier, New York, 392 p.

Moshier, S. O., and B. L. Kirkland, 1993, Identification and diagenesis of a phylloid alga: *Archaeolithophyllum* from the Pennsylvanian Providence Limestone, western Kentucky: Journal of Sedimentary Research, v. 63, p. 1032–1041.

Mount, J. F., 1984, The mixing of siliciclastic and carbonate sediments in shallow shelf environments: Geology, v. 12, p. 432–435.

Mullins, H. T., K. C. Heath, M. H. Van Buren, and C. R. Newton, 1984, Anatomy of a modern open ocean carbonate slope: northern Little Bahama Bank: Sedimentology, v. 31, p. 141–164.

Qing, H., and E. W. Mountjoy, 1994, Formation of coarsely crystalline, hydrothermal dolomite reservoirs in the Presqu'ile Barrier, Western Canada Sedimentary Basin: American Association of Petroleum Geologists Bulletin, v. 78, p. 55–77.

Radke, B. M., and R. L. Mathis, 1980, On the formation and occurrence of saddle dolomite: Journal of Sedimentary Research, v. 50, p. 1149–1168.

Ross, C. A., and J. R. P. Ross, 1987, Late Paleozoic sea levels and depositional sequences, *in* C. A. Ross and D. Haman, eds., Timing and depositional history of eustatic sequences, constraints on seismic stratigraphy: Cushman Foundation for Foraminiferal Research Special Publication 24, Ithaca, New York, p. 137–149.

Ross, C. A., and J. R. P. Ross, 1988, Late Paleozoic transgressive-regressive deposition, *in* C. K. Wilgus, B. S. Hastings, H. Posamentier, J. V. Wagoner, C. A. Ross, and C. G. St. C. Kendall, eds., Sea-level changes: An integrated approach: Society of Economic Paleontologists and Mineralogists Special Publication 42, Tulsa, Oklahoma, p. 227–247.

Ross, C. A., and J. R. P. Ross, 2003, Sequence evolution and sequence extinction: Fusulinid biostratigraphy and species-level recognition of depositional sequences, Lower Permian, Glass Mountains, West Texas, U.S.A., *in* H. C. Olson and R. M. Leckie, eds, Micropaleontologic proxies for sea-level change and stratigraphic discontinuities: Society of Economic Paleontologists and Mineralogists Special Publication 75, Tulsa, Oklahoma, p. 317–359.

Rygel, M. C., C. R. Fielding, T. D. Frank, and L. P. Birgenheier, 2008, The magnitude of Late Paleozoic glacioeustatic fluctuations: A synthesis: Journal of Sedimentary Research, v. 78, p. 500–511.

Saller, A. H., J. A. D. Dickson, and S. A. Boyd, 1994, Cycle stratigraphy and porosity in Pennsylvanian and Lower Permian shelf limestones, eastern Central Basin Platform, Texas: American Association of Petroleum Geologists Bulletin, v. 78, p 1820–1842.

Scholle, P. A., and D. S. Ulmer-Scholle, 2003, A color guide to the petrography of carbonate rocks: Grains, textures, porosity, diagenesis: American Association of Petroleum Geologists Memoir 77, Tulsa, Oklahoma, 459 p.

Spötl, C., and J. K. Pitman, 1998, Saddle (baroque) dolomite in carbonates and sandstones: a reappraisal of a burial-diagenetic concept, *in* S. Morad, ed., Carbonate cementation in sandstones: International Association of Sedimentologists Special Publication 26, p. 437–460.

Tucker, M. E., and V. P. Wright, 1990, Carbonate sedimentology; Blackwell Science, Oxford, U.K., 492 p.

Wahlman, G. P., 2002, Upper Carboniferous Lower Permian (Bashkiriane/Kungurian) mounds and reefs, *in* W. Kiessling, E. Flugel, and J. Golonka, eds., Phanerozoic reef patterns: Society of Economic Paleontologists and Mineralogists Special Publication 72, Tulsa, Oklahoma, p. 271–338.

Waite, L. E., 1993, Upper Pennsylvanian seismic sequences and facies of the eastern and southern Horseshoe Atoll, Midland

Basin, West Texas, *in* R. G. Loucks and J. F. Sarg, eds., Carbonate sequence stratigraphy: Recent developments and applications: American Association of Petroleum Geologists Memoir 57, Tulsa, Oklahoma, p. 213–240.

Wright, W. R., 2011, Pennsylvanian paleodepositional evolution of the greater Permian Basin, Texas and New Mexico: Depositional systems and hydrocarbon reservoir analysis: American Association of Petroleum Geologists Bulletin, v. 95, p. 1525–1555.

Yancey, T. E., 1986, Mixed carbonate-terrigenous clastic sedimentation on a ramp-topped shelf, (distally-steepened ramp), the eastern shelf on the Midland Basin: West Texas Geological Society Bulletin, v. 25, p. 4–10.

Yose, L. A., and P. L. Heller, 1989, Sea-level control of mixed-carbonate-siliciclastic, gravity-flow deposition: Lower part of the Keeler Canyon Formation (Pennsylvanian), southeastern California: Geological Society of America Bulletin, v. 101, p. 427–439.